ADVANCED FUNCTIONAL MATERIALS
www.afm-journal.de

Unilateral Asymmetric Radiation in Bilayer Metasurfaces

Junhao Tan, Ruhao Pan, Yuan Xiang, Zhiyang Tang, Bo Wang,* and Junjie Li**

Asymmetric radiation (AR) achieved by breaking the spatial symmetry of the metasurface has been widely concerned for its rich physics and broad prospect in micro/nano-optical devices. However, the AR on the same side of the metasurface is still hard to be realized limited by the spatial controllability of the nanostructures. Here, a bilayer metasurface composed of two layers of nanopillars with hexagonal lattice is engraved, and AR response is observed on the same side of the metasurface. By tailoring the shift between layers, the bound - state in the continuum (BIC) supported by the metasurface becomes quasi-BIC. Meanwhile, the far-field polarization of the quasi-BICs with in-plane wave-vectors $k_{\|}$ are different from those with $-k_{\|}$ wave-vectors, meaning that the transmissions on the same side of the metasurface but of light with opposite incident angles are different ($T(k_{\|}) \neq T(-k_{\|})$), indicating a new type of AR and is called unilateral AR (UAR). The asymmetric transmission is verified by experiments of bilayer metasurface with shifts, and a maximum difference of 0.1 can be obtained. This work reveals a new type of AR and enables the design of a series of functional nano-optical devices including on-chip lasers and energy-efficient couplers.

1. Introduction

Asymmetric radiation (AR), which refers to a radiation difference of light from opposite directions of systems, has attracted tremendous concerns for controlling lights. Optical devices with AR have been proven to be potentially used in the fields of non-Hermitian physics[1] and singular optics,[2] such as on-chip lasers[3] and energy-efficient grating couplers.[4] Successful attempts including structures of multilayer films,[5] gratings[6] and even Mie scatters[7] have been reported with AR based on various mechanisms such as the tunneling effect of unidirectional surface plasmon polaritons,[8] Kerker condition,[9] and cross-polarization conversion.[10] The AR is usually achieved by introducing spatial symmetry breaking.[11] Metasurfaces consisting of subwavelength resonators have been studied systemically in recent years[12] and are an excellent platform for symmetry breaking, providing a flexible possibility for AR for one can design their spatial configuration on demand and easy to break the symmetry. For example, a chiral metasurface[13] has reported with AR of circular response for its asymmetric configuration.

Previous reports on AR of metasurfaces are usually classified into two types. First, the transmittance is different between the forward and backward incidence of light.[6c,14] Second, guided-modes resonances (GMRs) in photon crystal slabs leak asymmetrically into the upper and lower cladding.[6a,14d,15] Two phenomena are closely related to symmetry breaking. The above-mentioned AR corresponds to the different radiations on the different sides of the devices. But when it comes to the AR where the radiations of the same side of the metasurface are different about opposite in-plane wavevectors ($\boldsymbol{k}_{\|}$), although there is evidence show that the asymmetric configuration can achieve this capacity,[13] a systemic discussion of its mechanism and modulating strategy is still lacking. We call this type of AR as unilateral AR (UAR). It might be counterintuitive because the resonant frequencies and damping rates must remain the same for radiate with opposite $\boldsymbol{k}_{\|}$ according to the time-reversal symmetry. However, their polarization states can be different when the metasurfaces have certain spatial symmetry breaking.[15] In this way, the coupling rates between the incident light with fixed polarization and radiate with opposite $\boldsymbol{k}_{\|}$ are different, and asymmetric transmission might happen. Bound-states in the continuum (BICs), which refers to a special class of nonradiative electromagnetic eigenmodes with no resonance linewidth and show irreplaceable potentials in sensing, lasing, and beam shaping, have become a new star in nanophotonics fields.[16] Symmetry breaking can produce quasi-BIC (q-BIC) with finite high quality factor (Q-factor) and finite resonance linewidth, which can be used to engineer polarization states, especially polarization vortices of radiate in the momentum space.[17] Hence, the BIC metasurface has become a most hopeful candidate for the realization of UAR.

In this work, we proposed a bilayer metasurface that is composed of two identical layers of a hexagonal lattice of nanopillars to achieve the UAR, which is characterized by the transmission difference on the same side of the metasurface but of opposite illuminated angle. When both layers of the metasurface are aligned with each other, a BIC can be observed

J. Tan, R. Pan, Y. Xiang, Z. Tang, B. Wang, J. Li
Beijing National Laboratory for Condensed Matter Physics
Institute of Physics
Chinese Academy of Sciences
Beijing 100190, China
E-mail: panruhao@iphy.ac.cn; wangbo2014@iphy.ac.cn; jjli@iphy.ac.cn
J. Tan, Y. Xiang, Z. Tang, J. Li
School of Physical Sciences
University of Chinese Academy of Sciences
Beijing 100049, China

The ORCID identification number(s) for the author(s) of this article can be found under https://doi.org/10.1002/adfm.202501156

DOI: 10.1002/adfm.202501156

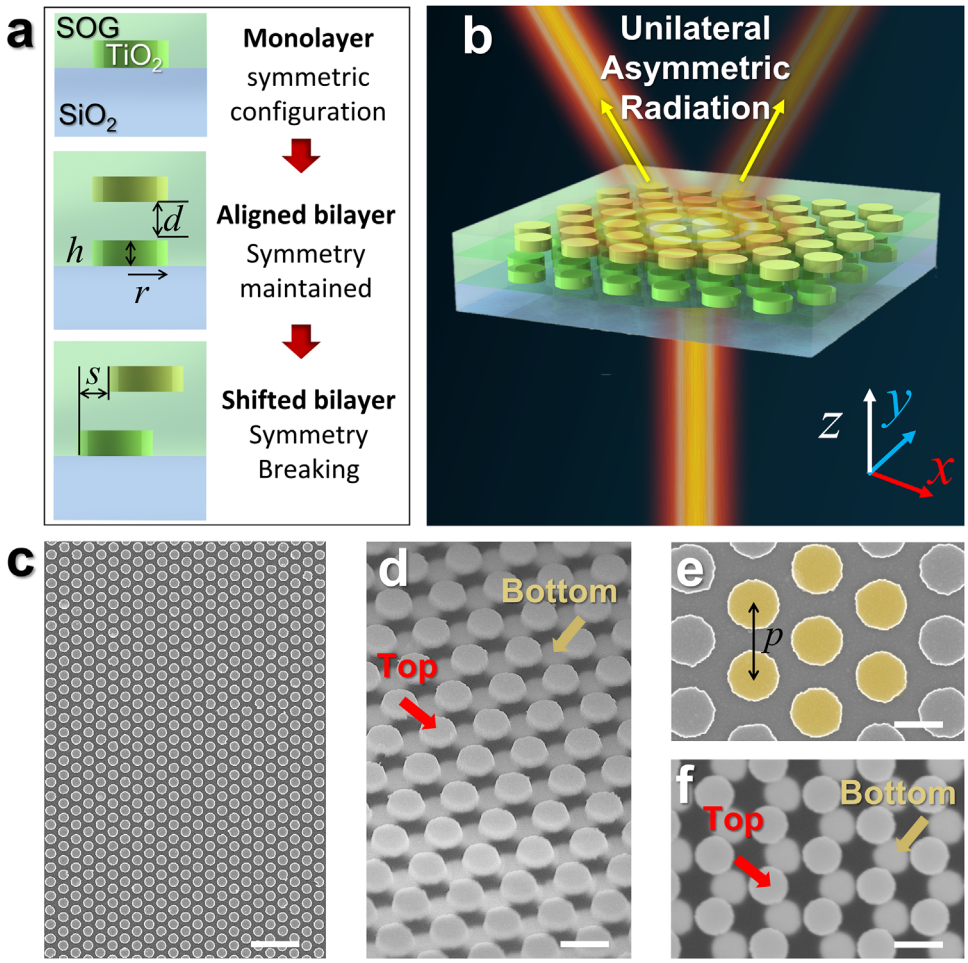

Figure 1. The design and the fabrication of the bilayer metasurfaces. a) Schematics of the configuration and symmetry of the monolayer unit cell, the bilayer unit cell without and with shift, where the radius and the height of the radius are labeled as *r* and *h*, and the distance and the shift between layers are labeled as *d* and *s*, respectively. b) Schematic diagram of bilayer metasurface and asymmetric radiation capacity. c) Large area SEM image of the single-layer lattice. d) Tilted view of bilayer metasurface. e) and f) top views of the details of single-layer lattice and bilayer metasurface with a certain shift. Scale Bar: (c) 3 μm, (d) and (f) 0.4 μm, and (e) 0.3 μm.

with no UAR for the spatial symmetry is unbroken in this regime. Temporal coupled-mode theory, which is a powerful tool for the investigation of energy propagation and mode coupling of the optical system,[18] demonstrates that the breaking of both the C_2 symmetry and up-down mirror symmetry is essential in achieving UAR. Thus, we further introduce a shift between the layers to break the spatial symmetry, from which, the far-field polarization states in *k*-space are redistributed due to the evolution of BIC to q-BIC. Specially, the polarization states of the q-BICs at $\boldsymbol{k}_{\parallel}$ are found to be very different from those at $-\boldsymbol{k}_{\parallel}$, which results in UAR. The UAR has been experimentally validated by measuring angular resolved transmission spectra, where asymmetric transmission at the q-BICs is observed. Our work on UAR, where the transmission difference can be observed from the same side of the metasurface, is an important supplement to AR from the aspect of radiation direction. It gives a new idea of modulating light and helps the design of a series of micro/nano-optical devices.

2. Results and Discussion

Figure 1 shows the concept of bilayer metasurfaces to achieve the UAR. As Figure 1a shows, as for a single layer composed of an array of circular TiO_2 nanopillar surrounded by spin-on-glass (SOG), whose radius and height are labeled as *r* and *h*, on the quartz substrate, the light experiences a uniform media along the *z*-direction, and mirror symmetry exists in the *x*-*y* plane. When it comes to a bilayer nanostructure with a spacer of $d = 100$ nm and the centers of the two layers coincide, the symmetry is still maintained compared with the single layers. Then, a shift (labeled as "*s*") is further introduced into the bilayer system, by which both in-plane and out-of-plane symmetry breaking is achieved.

A bilayer metasurface is then realized by two layers of the hexagonal array with a certain shift. Figure 1b shows schematically the UAR capacity of the bilayer metasurface, where polarized lights with opposite incident angles against the surface normal show different intensities. Here, we choose TiO_2 as the material of the nanopillar for its high index and low

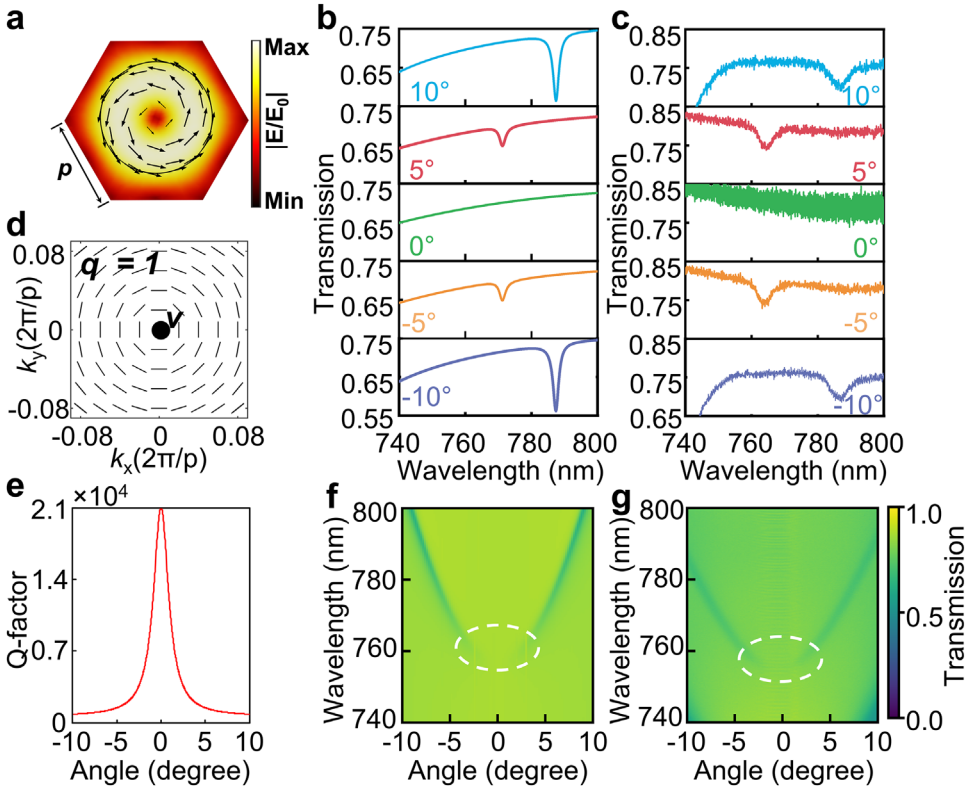

Figure 2. Optical response of bilayer metasurface. a) Electric field distribution of a unit cell in the array along the *x*-*y* plane. b) and c) Simulated/experimental spectra with different incident angles. d) Far-field polarization distribution in *k*-space. e) The Q-factor of the eigenmode versus the incident angle. f) and g) The simulated and experimental spectra with changed incidence angle.

intrinsic loss in the visible band (Figure S1, Supporting Information). While SOG is the surround for its similar index to quartz, which helps to avoid the interferometric fringe during the measurement. One can regard the bilayer metasurface to be entirely immersed in a dielectric circumstance of $n = 1.46$.

The metasurface is fabricated by the planar micro/nanofabrication. The detailed fabrication procedures are described in Figure S2 (Supporting Information). Both the efficiency of the UAR and the fabrication feasibility are considered to determine the feature sizes of the unit cell, which are discussed in detail in Figure S3 (Supporting Information). Finally, the radius, height, and the period of the nanopillar in the hexagonal lattice have been fixed as $r = 180$ nm, $h = 100$ nm, and $p = 519$ nm, which is further fabricated by the method displayed in Figure S2 (Supporting Information). Figure 1c,d depict the large area view of the single layer of nanopillar array and the tilt view of the bilayer metasurface, where structures in the metasurface have a uniform shape. Their enlarged views are further demonstrated in Figure 1e,f, indicating the fabricated and the designed key features are in good consistency, and the pitch of the array is observed to be $p = 519$ nm, which is in good consistency with the design. The out-of-plane asymmetric degree of the bilayer metasurface can be tailored by the shift between the layers. Thus, AR metasurfaces with various *s* are fabricated and their scanning electron microscope (SEM) images can be found in Figure S4 (Supporting Information), the distinctive morphologies of the metasurface demonstrate that the out-of-plane asymmetry is modulated.

According to the above-mentioned design, the optical response of the bilayer of the hexagonal circle lattice with $s = 0$ is discussed first. **Figure** 2a shows the electric field distribution $\boldsymbol{E}$(x,y) in the unit cell on the *x*-*y* plane. One can see that $\boldsymbol{E}(x,y)$ has even parity against the C_2 rotation operation, indicating a symmetry-protected BIC. The angular resolved transmission spectra are presented in Figure 2b (simulation) and Figure 2c (measurement). There is no obvious resonance that can be observed from the curves of normal incidence, but a dip is found once the incident light is tilted. With the detection angle increasing, the dip shows a redshift from 755 to 787 nm (incident angle of 10°), and the full-width half maxima (FWHM) broaden, while the spectra are symmetric for the same incident angle of opposite direction. The resonance wavelength is not a diffraction wavelength and is far away from that of other eigenmodes, thus the influence of the high-order modes or parasitic modes on the transmission can be ignored. Both the simulation and experiment confirm the spectrum evolution trend. In Figure 2d, from the perspective of polarization distribution of the far-field radiation in *k*-space, the metasurface hosts a BIC at the Γ-point with a topological charge of $q = 1$, which is accompanied by a polarization singularity surrounded by linear polarization. When the in-plane wavevector $\boldsymbol{k}_{\parallel}$ deviates from the center of the Brillouin zone, the bound states can leak radiation out and external light can interact with the resonance. Hence, the Q-factor decreases from an infinite to a

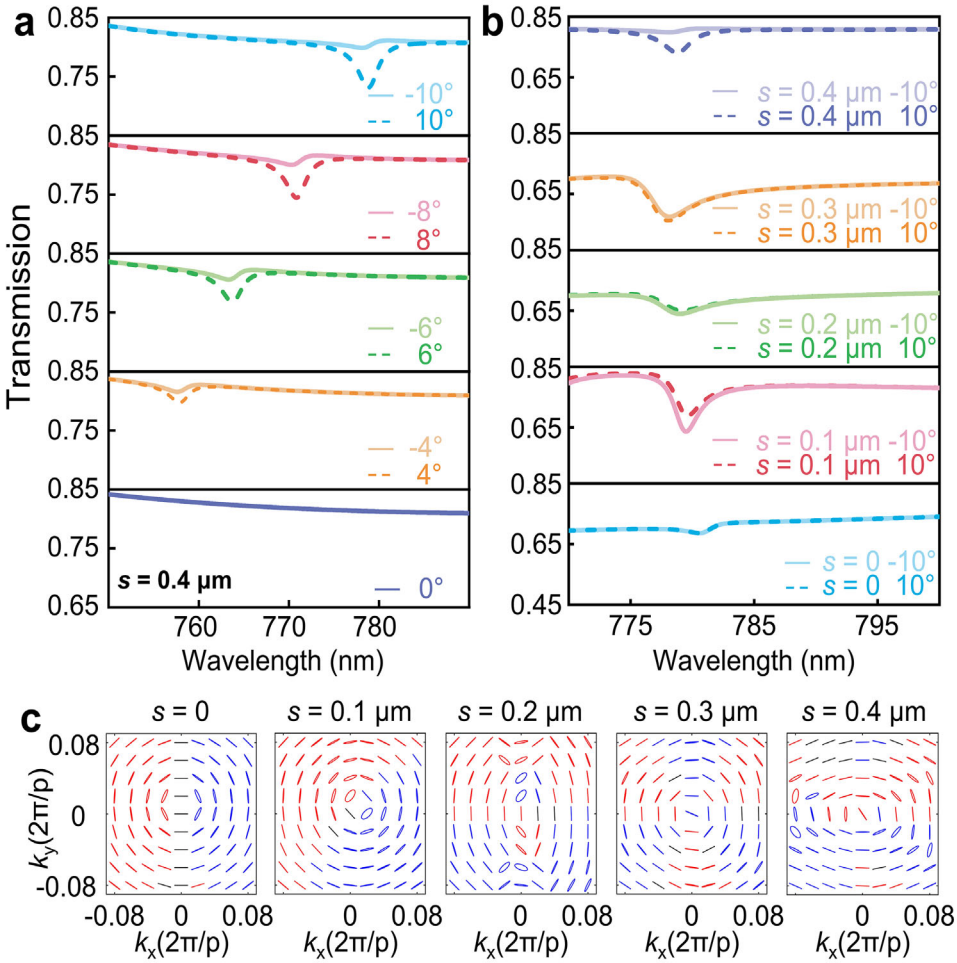

Figure 3. Simulated spectra and far-field polarization distribution of bilayer metasurface with different shift. a) The transmitted spectra of different incident angles at the shift of 0.4 μm. b) The spectra of different shifts at the same incident angle. c) The simulated polarization distribution of the far-field radiation with different shifts.

finite value. Figure 2e shows the variation trend of the Q-factor with the incident angle, the Qactor exponentially increases with the decrease of the incident angle, showing the infinite Q-factor of BIC. Figure 2f,g demonstrate the simulated and experimental 2D spectra of the bilayer with no shift between each other, respectively, in which the redshift and the Q-factor change with the incident angle are intuitively observed. What's more, both simulation and experiment show a gap along the BIC band for vertical illumination, meaning that the Q-factor of BIC mode is rather large and cannot be distinguished.[19]

Although BIC mode can be achieved in bilayer metasurface with no shift, the transmission is symmetric with the incident angle. Here, we introduce a shift between the layers to break both in-plane and out-of-plane symmetry, where the shift along the *y*-axis is 10 nm while that along the *x*-axis is changed and labeled as "*s*". By setting $s = 400$ nm, the transmitted spectra of the bilayer metasurface with different incident angles are simulated and shown in **Figure** 3a, where the in-plane wavevector $\boldsymbol{k}_{\parallel}$ of the incident light is along the *x*-axis and its polarization is along the *y*-axis. As for the normal incidence, no dip can be found in the transmitted curve, while once a slant angle is applied to the incidence, a dip that is dependent on the incident angle can be distinguished, indicating there is a BIC mode in this bilayer system. Where the incident angle labeled with the symbol "-" refers to right-tilt incidence, while that with no label indicates left-tilt one. The intensity of the dip is distinct with incident light of opposite tilt angle. The transmission difference for incident light of different directions is generally enhanced with the tilt angle and reaches 0.07 for an angle of 10°. Moreover, the redshift of the dip from 755 (0°) to 778 nm (10°), the UAR on both sides is finally realized by bilayer metasurface.

There is no doubt that the shift between the two layers of the metasurface determines the degree of asymmetry of the optical system. To emphasize the role of the shift on the AR, we have simulatively investigated the angle resolution transmitted spectra of metasurfaces with different shifts. By setting 10° as the incident angle, Figure 3b shows the spectra of shift that changes from 0 to 0.4 μm from bottom to top. Not surprisingly, the spectra are perfectly overlapped for the metasurface with no shift. As for the bilayer with a shift, when the shift is set to 0.1 and 0.2 μm, the light collected from the left side is larger than that of the right one. Despite the transmission differences being distinctive, this

trend is reversed for the shift of 0.3 and 0.4 μm, namely the collected light from the left side is smaller than the right. The transmission difference is complicated with the shift, showing what has a far-reaching influence on the BIC.

The simulated polarization distribution of the far-field radiation with different shifts is also shown in Figure 3c, which presents the intrinsic polarization profile at the same *k*-space location. On the polarization profile, the polarization states are represented by ellipses, where blue and red colors represent the left-handed and right-handed states, respectively. As for the metasurface with $s = 0$ but a shift of 10 nm is introduced to the *y*-axis, the elliptical polarization can be found near the Γ point, meaning that the small shift along the *y*-axis brings a basement of circular optical response. With the increase of *s*, chirality begins to change gradually. When $s = 0.1$ and 0.2 μm, the polarized states show obvious asymmetry on both sides of the Γ point, indicating the existence of UAR. When $s = 0.3$ μm, the far-field polarization becomes more symmetric due to the structure being close to a symmetric one (Figure S4, Supporting Information), and thus the angle-resolved transmitted spectra do not show different curves. With the *s* increase continuously, the spatial asymmetry is enlarged, and dramatical differences of polarization on both sides of Γ point can be distinguished. For instance, the polarized state at the $\boldsymbol{k}_x = 0.08$, $\boldsymbol{k}_y = 0$ and $\boldsymbol{k}_x = -0.08$, $\boldsymbol{k}_y = 0$ show various ellipticity, indicating the polarization states of the q-BICs at $\boldsymbol{k}_{\parallel}$ are found to be very different from those at $-\boldsymbol{k}_{\parallel}$, and in turn, the transmissions on the same side of the metasurface but with incidence of opposite incident angles are different ($T(\boldsymbol{k}_{\parallel}) \neq T(-k_{\parallel})$, which results in a strong UAR. The influence of the interlayer distance on the UAR and the Q-factor are also simulated and investigated, one can refer to Figure S5 (Supporting Information), which shows the intensity of UAR decreased, while the Q-increased with the distance between layers, for details. Temporal coupled-mode theory (TCMT) is further introduced to highlight the importance of spatial symmetric breaking[20] (see Supporting Information). It can be seen that for the metasurface with C_2 symmetry, the coefficient matrix $D(\boldsymbol{k}_{\parallel})$ satisfies:

$$D\left(-k_{\parallel}\right) = e^{i\varphi} D\left(k_{\parallel}\right) \tag{1}$$

where φ is an arbitrary phase, indicating that the incident light with opposite in-plane wavevectors has the same coupling coefficients despite a phase delay. If mirror symmetry in the *z*-*y* plane is maintained, the transmission of the *s*-polarized light can be written as:

$$T_{ss}\left(k_{\parallel}\right) = t_s - \frac{\pm d_s\left(k_{\parallel}\right) d_s\left(-k_{\parallel}\right)}{i\left(\omega - \left(\omega_0 + i\gamma\right)\right)} \tag{2}$$

where t_s refers to the transmission coefficient of nonresonant position, ω and $\omega_0 + i\gamma$ are the frequency of the incidence and complex eigenfrequency. One can Figure out that $T_{ss}(\boldsymbol{k}_{\parallel})$ always equals $T_{ss}(-\boldsymbol{k}_{\parallel})$. A similar result can be obtained for T_{pp}. Indicating that breaking both the C_2 rotation symmetry and up-down mirror symmetry is necessary for the observation of asymmetric transmission.

Following the simulation, the metasurface with a bilayer configuration is then fabricated by e-beam lithography and the pattern transfer processes. The transmitted spectra for the metasurfaces with different shifts are collected in **Figure** 4a, where no dip can be found for the vertical incidence. But dips with opposite direction incidences are obtained, and the transmission difference is increased with the incident angle. Despite the redshift, the modulation depth of the resonance is increased with the tilted angle for left side incidence but decreased with right side incidence, verifying that the AR of out-of-plane asymmetry that origins from the asymmetric polarization distribution in the *k*-space. There is another resonance on the high-frequency band showing the UAR phenomenon. To Figure out the origin of the high frequency UAR, Figure S6 (Supporting Information) shows the optical response of the single layer of a hexagonal lattice, where a BIC can be found at 720 nm and redshift to 750 nm with the incident angle, which is consistent with the wavelength of high frequency UAR in the bilayer. Notably, the UAR response cannot be found in the single layer, meaning that the interaction of the BIC by overlapping the layers leads to the UAR for the bilayer metasurface with shift. We further fix an incident angle of 10° but vary the shift of the bilayer, and spectra are obtained and depicted in Figure 4b. Despite the overlapping curve for vertical incidence. As the shift increases, the amplitude of the incident light on the left side is first smaller than that on the right side, and then larger than the right side, which is consistent with the simulation. Figure 4c is the angle resolution spectra of the bilayer metasurface. The left panel shows the spectrum for $s = 0$, and the right panel is the spectrum for $s = 0.4$ μm. Compared to the symmetric transmission of symmetric nanostructures, obvious asymmetric transmittance can be found for bilayer metasurface with no spatial symmetry, and asymmetric transmission always exists with tilt incidence. By set the intensity of UAR as the transmission difference of the opposite angle incidence. Figure 4d statistics the intensity of UAR under different shifts. It can be seen that the simulation and the experiment are in the same evolution trend, and a maximum of 0.1 can be found for the shift of 400 nm. Figure 4e depicts the UAR of opposite incident angles when $s = 0.4$ μm, which shows an increasing trend of UAR. The differences between the simulation and the experiment come from the imperfection of the experiment. The inconsistency between the experiment and the simulation mainly comes from the imperfection of fabrication and the measurement, for example, the fabrication precision of EBL, uniformity of the SOG layer, and the inevitable roughness of the structures' surface. Moreover, the UAR of the bilayer metasurface for *x*-polarized incidence is also investigated and shown in Figure S7 (Supporting Information). Although the transmission becomes weaker for *x*-polarization incidence, both the evolution trend and the intensity of the UAR are highly consistent with that of *y*-polarized incidence.

It should be noted that the intensity of the UAR can be further enhanced by optimizing the sizes of the structures, the shape of the unit cells, and the materials of the bilayer metasurface. For example, we have constructed a metasurface of a rectangular unit cell. The results can be found in the supporting information (Figure S8, Supporting Information), similar properties with the bilayer metasurface of circle nanopillar can be found in the rectangle metasurface, and the UAR origins from the spatial asymmetry rather than the detailed configuration of the building block. A higher AR of 0.14 can be obtained for the bilayer metasurface with the rectangle nanopillar.

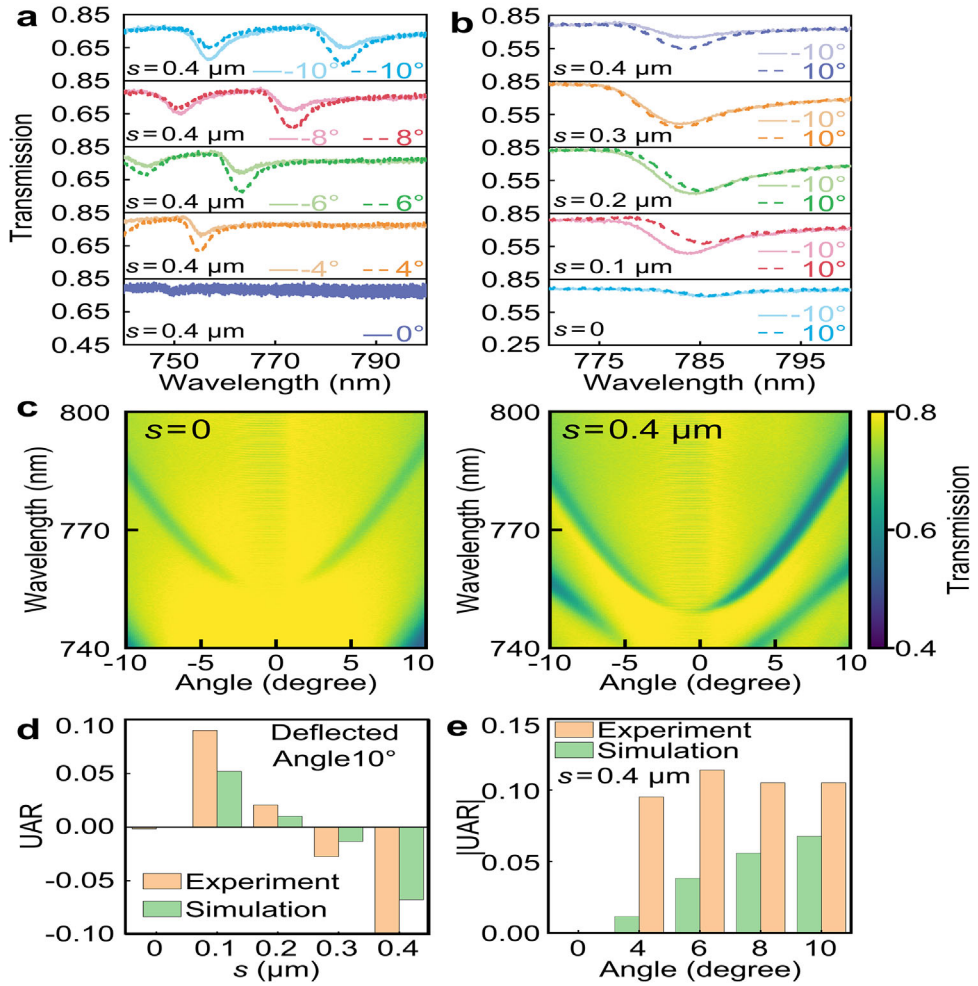

Figure 4. The experimental demonstration of UAR. a) The transmitted spectra of the metasurface with $s = 0.4$ μm and different incident angles, and the spectra of different shifts at incident angle 10° are shown in b). c) 2D transmission map about incident angle for metasurface with $s = 0$ (left) and $s = 0.4$ μm (right). d) and e) The change of intensity of UAR with the shift and incident angle, respectively.

3. Conclusion

In conclusion, we brought a bilayer metasurface of two layers of hexagonal lattice to achieve the UAR, where its behind physics and modulation have been systemically discussed, namely the UAR results from the symmetric breaking of far-field polarization distribution in the *k*-space of the BIC hosted by the bilayer. Thanks to the shift of the bilayer metasurface results in a spatial symmetry breaking, the far-field polarization states in the *k*-space are asymmetric for a couple of opposite tilted angles is distinctive, and thus the UAR is obtained. Both the simulation and the experiment confirm the existence of UAR, showing it is increased with the tilt angle of incidence and is dependent on the shift between the layers, a difference of 0.1 is observed for 400 nm shift and 10° tilt incident beam. Research on the bilayer metasurfaces with different resonators shows that the UAR originates from the shift of the special lattice arrangement of the bilayer metasurface rather than the configuration detail of the build blocks. Our results bring a new type of asymmetric radiation, which deserves further study to inspire a series of fresh mechanisms and optical devices.

4. Experimental Section

Fabrication: The bilayer system was fabricated by a simple alignment lithography method and the fabrication process was schematically depicted in Figure S2 (Supporting Information). The quartz was chosen as the substrate. First, a layer of polymethyl methacrylate (PMMA 495A5) with 200 nm in thickness was spin-coated at 4000 rpm and prebaked at 180 °C for 1 min for hardening. EBL (EBPG 5200, Raith) was utilized to expose the align marker of 20 μm × 20 μm square in shape. Following, 50 nm Au was further deposited by electron beam evaporation (EBE, FU-12PEB) after development, and the mark was then prepared by a lift-off process. Then, the 100 nm-thick TiO_2 layer was deposited by the atomic layer deposition (ALD, Savannah G2). PMMA was spin-coated in the same way mentioned before. The pattern of the bottom layer was directly written and developed by the alignment EBL. After that, the PMMA pattern was transferred to a Cr pattern with 50 nm in thickness by EBE and the following lift-off process. Afterward, TiO_2 was etched by inductively coupled plasma reactive ion etching (ICP-RIE, LEUVEN Haasrode Pishow A) with

Cr as the mask. Immersed the sample into chromium etchant for 10 min to completely corrode the residual Cr film. Finally, the bottom layer of the metasurface was constructed after coating a layer of spin of glass (SOG) with 200 nm in thickness by 3000 rpm spin-coating and baking at 200 °C for 2 min to cover the first layer of TiO_2 nanopillar. The fabrication of the top layer was a complete repeat of the fabrication of the bottom layer, and only the displacement in alignment lithography affects the size of the shift.

Simulation: The finite element method (FEM) method was used to simulate electromagnetic fields, transmission, and the far-field polarization distribution of the metasurface. All model was set up using rectangular periods, each of which contains two metaatoms. The 3D model of the unit cell was built up and simulated with periodic boundary conditions along the *x* and *y*-axis and perfectly matched layers (PML) along the propagation of electromagnetic waves (*z*-axis). The Floquet period was used, the *k* vectors are:

$$\begin{cases} k_x = \frac{2\pi}{p} m \\ k_y = \frac{2\pi}{p} n \end{cases} \quad m = [-0.1, 0.1], n = [-0.1, 0.1]. \tag{3}$$

where *p* is a value with a unit of 1/m, *m*, and *n* are independent variables indicating different positions in the momentum space. The PMLs of 100 nm were introduced both on the top and the bottom of the model. The unit cell sits in the middle of the model. A layer of air/SiO_2 with a height of 1 µm was added on/under the structures. Material properties in Figure S1 (Supporting Information) were used for material settings.

Optical Characterization: The angle-resolved micro-area spectrometer (ARMS, Ideaoptics) was used to collect angle-resolved transmission spectra, which was a type of mature scientific equipment. The whole operating band of the equipment was 400 to 1650 nm, here the collected waveband was chosen by a high-resolution monochromator (Princeton Instruments, HRS 300) from 700 to 800 nm, the signal of the light source was collected from a quartz substrate and the background signal was collected by covering the light source with a shutter. The polarizer can be plugged into the system to generate polarized light on demand. During the test, an aperture was introduced to select a 100 µm × 100 µm area for measurement, both the polarized and unpolarized light illuminated the selected area from the back, and a 100× (NA = 0.9) objective was introduced to collect the outputted signal, following by the signal was recorded by a charge-coupled device (CCD).

Supporting Information

Supporting Information is available from the Wiley Online Library or from the author.

Acknowledgements

This work was supported by the National Key Research and Development of China (Grant Nos. 2023YFF0715902 and 2023YFF0721901), the National Natural Science Foundation of China (Grant Nos. 12074420, U21A20140, 12304463, and 12204527), the Chinese Academy of Sciences through the Project for Young Scientists in Basic Research (YSBR-021). This work is also technically supported by the Beijing Metasurface Optics Device Generic Technology Platform, Synergetic Extreme Condition User Facility (SECUF, https://cstr.cn/31123.02.SECUF) and China and IOP-HKUST-Joint Laboratory for Wave Functional Materials Research.

Conflict of Interest

The authors declare no conflict of interest.

Data Availability Statement

The data that support the findings of this study are available from the corresponding author upon reasonable request.

Keywords

bilayer metasurfaces, bound states in the continuum, symmetry breaking, unilateral asymmetric radiation

Received: January 13, 2025
Revised: April 10, 2025
Published online:

[1] a) D. Leykam, K. Y. Bliokh, C. Huang, Y. D. Chong, F. Nori, *Phys. Rev. Lett.* **2017**, *118*, 040401; b) H. Shen, B. Zhen, L. Fu, *Phys. Rev. Lett.* **2018**, *120*, 146402.
[2] a) M. Soskin, S. V. Boriskina, Y. Chong, M. R. Dennis, A. Desyatnikov, *J. Opt.* **2017**, *19*, 010401; b) M. V. Berry, *Light: Sci. Appl.* **2023**, *12*, 238.
[3] a) H. Matsubara, S. Yoshimoto, H. Saito, Y. Jianglin, Y. Tanaka, S. Noda, *Science* **2008**, *319*, 445; b) M. Yoshida, M. De Zoysa, K. Ishizaki, Y. Tanaka, M. Kawasaki, R. Hatsuda, B. Song, J. Gelleta, S. Noda, *Nat. Mater.* **2019**, *18*, 121.
[4] a) G. Roelkens, D. V. Thourhout, R. Baets, *Opt. Lett.* **2007**, *32*, 1495; b) H. Cho, S. Moon Kim, Y. Sik Kang, J. Kim, S. Jang, M. Kim, H. Park, J. Won Bang, S. Seo, K.-Y. Suh, Y.-E. Sung, M. Choi, *Nat. Commun.* **2015**, *6*, 8484.
[5] Y. D. Chong, L. Ge, H. Cao, A. D. Stone, *Phys. Rev. Lett.* **2010**, *105*, 053901.
[6] a) X. Yin, J. Jin, M. Soljačić, C. Peng, B. Zhen, *Nature* **2020**, *580*, 467; b) H. Qin, S. Chen, W. Zhang, H. Zhang, R. Pan, J. Li, L. Shi, J. Zi, X. Zhang, *Nat. Commun.* **2024**, *15*, 9080; c) Z.-P. Zhuang, H.-L. Zeng, X.-D. Chen, X.-T. He, J.-W. Dong, *Phys. Rev. Lett.* **2024**, *132*, 113801.
[7] M. V. Gorkunov, A. A. Antonov, V. R. Tuz, A. S. Kupriianov, Y. S. Kivshar, *Adv. Opt. Mater.* **2021**, *9*, 2100797.
[8] J. Ho, Y. H. Fu, Z. Dong, R. Paniagua-Dominguez, E. H. H. Koay, Y. F. Yu, V. Valuckas, A. I. Kuznetsov, J. K. W. Yang, *ACS Nano* **2018**, *12*, 8616.
[9] a) J. M. Geffrin, B. García-Cámara, R. Gómez-Medina, P. Albella, L. S. Froufe-Pérez, C. Eyraud, A. Litman, R. Vaillon, F. González, M. Nieto-Vesperinas, J. J. Sáenz, F. Moreno, *Nat. Commun.* **2012**, *3*, 1171; b) M. Decker, I. Staude, M. Falkner, J. Dominguez, D. N. Neshev, I. Brener, T. Pertsch, Y. S. Kivshar, *Adv. Opt. Mater.* **2015**, *3*, 813; c) A. I. Kuznetsov, A. E. Miroshnichenko, M. L. Brongersma, Y. S. Kivshar, B. Luk'yanchuk, *Science* **2016**, *354*, aag2472.
[10] M. Kang, Z. Zhang, T. Wu, X. Zhang, Q. Xu, A. Krasnok, J. Han, A. Alù, *Nat. Commun.* **2022**, *13*, 4536.
[11] X. Ni, Y. Liu, B. Lou, M. Zhang, E. L. Hu, S. Fan, E. Mazur, H. Tang, *Phys. Rev. Lett.* **2024**, *132*, 073804.
[12] a) X. Zhao, Z. Sun, L. Zhang, Z. Wang, R. Xie, J. Zhao, R. You, Z. You, *Adv. Devices Instrum.* **2022**, *2022*, 9765089; b) M. Choi, J. Park, J. Shin, H. Keawmuang, H. Kim, J. Yun, J. Seong, J. Rho, *npj Nanophotonics* **2024**, *1*, 31; c) Y. Yang, J. Seong, M. Choi, J. Park, G. Kim, H. Kim, J. Jeong, C. Jung, J. Kim, G. Jeon, K.-i. Lee, D. H. Yoon, J. Rho, *Light: Sci. Appl.* **2023**, *12*, 152; d) C. Jung, G. Kim, M. Jeong, J. Jang, Z. Dong, T. Badloe, J. K. W. Yang, J. Rho, *Chem. Rev.* **2021**, *121*, 13013; e) Y. Yang, E. Lee, Y. Park, J. Seong, H. Kim, H. Kang, D. Kang, D. Han, J. Rho, *ACS Nano* **2025**, *19*, 3008.
[13] D. Gromyko, S. An, S. Gorelik, J. Xu, L. J. Lim, H. Y. L. Lee, F. Tjiptoharsono, Z.-K. Tan, C.-W. Qiu, Z. Dong, L. Wu, *Nat. Commun.* **2024**, *15*, 9804.
[14] a) S. Zhang, Y. Hu, G. Lin, Y. Niu, K. Xia, J. Gong, S. Gong, *Nat. Photonics* **2018**, *12*, 744; b) X. Guo, Y. Ding, Y. Duan, X. Ni, *Light: Sci. Appl.* **2019**, *8*, 123; c) X. Huang, C. Lu, C. Liang, H. Tao, Y.-C. Liu, *Light: Sci. Appl.* **2021**, *10*, 30; d) X. Yin, T. Inoue, C. Peng, S. Noda, *Phys. Rev. Lett.* **2023**, *130*, 056401.

[15] H. Zhou, B. Zhen, C. W. Hsu, O. D. Miller, S. G. Johnson, J. D. Joannopoulos, M. Soljačić, *Optica* **2016**, *3*, 1079.
[16] a) C. W. Hsu, B. Zhen, A. D. Stone, J. D. Joannopoulos, M. Soljačić, *Nat. Rev. Mater.* **2016**, *1*, 16048; b) S. Xiao, T. Liu, X. Wang, X. Liu, C. Zhou, *Phys. Rev. B* **2020**, *102*, 085410.
[17] a) D. C. Marinica, A. G. Borisov, S. V. Shabanov, *Phys. Rev. Lett.* **2008**, *100*, 183902; b) L. Huang, W. Zhang, X. Zhang, *Phys. Rev. Lett.* **2022**, *128*, 253901.
[18] a) A. Overvig, S. A. Mann, A. Alù, *Light: Sci. Appl.* **2024**, *13*, 28; b) G. Alagappan, F. J. García-Vidal, C. E. Png, *Phys. Rev. Lett.* **2024**, *133*, 226901.
[19] Y. Chen, H. Deng, X. Sha, W. Chen, R. Wang, Y.-H. Chen, D. Wu, J. Chu, Y. S. Kivshar, S. Xiao, C.-W. Qiu, *Nature* **2023**, *613*, 474.
[20] T. Yoda, M. Notomi, *Phys. Rev. Lett.* **2020**, *125*, 053902.